Applied Physics Letters ARTICLE scitation.org/journal/apl

Theoretical prediction of a highly responsive material: Spin fluctuations and superconductivity in $FeNiB_2$ system

Cite as: Appl. Phys. Lett. **115**, 182601 (2019); doi: 10.1063/1.5124489
Submitted: 14 August 2019 · Accepted: 18 October 2019 ·
Published Online: 30 October 2019

Renhai Wang,[1,2] Yang Sun,[2,a)] Vladimir Antropov,[2,a)] Zijing Lin,[1] Cai-Zhuang Wang,[2,3] and Kai-Ming Ho[2,3,4]

AFFILIATIONS

[1]Department of Physics, University of Science and Technology of China, Hefei 230026, China
[2]Ames Laboratory, US DOE, Ames, Iowa 50011, USA
[3]Department of Physics, Iowa State University, Ames, Iowa 50011, USA
[4]International Center for Quantum Design of Functional Materials (ICQD), Hefei National Laboratory for Physics Sciences at the Microscale, University of Science and Technology of China, Hefei 230026, China

[a)]**Electronic addresses:** yangsun@ameslab.gov and antropov@ameslab.gov

ABSTRACT

By analyzing the Fe-Ni-B compositional diagram, we predict an energetically and dynamically stable $FeNiB_2$ compound. This system belongs to the class of highly responsive state of materials, as it is very sensitive to the external perturbations. This state is also characterized by a high level of spin fluctuations, which strongly influence possible magnetic long- and short-range orders. Furthermore, we demonstrate that these antiferromagnetically dominating fluctuations could lead to the appearance of spin mediated superconductivity. The obtained results suggest a promising avenue for the search of strong spin fluctuation systems and related superconductors.

Spin fluctuations (SFs) in itinerant electron magnets play an important role in many metallic systems including weak itinerant magnets, heavy fermion compounds, actinides, Invar alloys, and many magnetoresistive materials. SFs also have been identified in high-temperature superconductors[1] and recently discovered Fe-based superconductors[2] with a clear suggestion about their crucial influence on the mechanisms of unconventional superconductivity. In the majority of cases, superconductivity appears near the magnetic quantum critical point, where magnetism has a pure itinerant character with no local moments involved. This is exactly a case when quantum SFs (including spin zero-point motion) are strong and provide a dominating contribution to many observable physical properties. However, as a typical example, in a case of superconductivity, the direct calculations and prediction of critical temperature from first principles are still not possible. In this situation, one can focus on searching for materials with a strong level of SF, leading to the possible development of promising physical properties.

Here, we will introduce qualitatively the concept of a highly responsive state (HRS) (see Fig. 1). This term is used here to indicate that a physical system is in a state characterized by an order parameter, which is very sensitive to the external perturbations (pressure, magnetic fields, etc.). The HRS is naturally related to closeness to the instability and, as usual in such situations, one can expect that fluctuations are very important.

To search for material of such type, we start our study with a less known system Fe-Ni-B in the concentration regime where magnetism is not supposed to be very strong (equal concentration of magnetic 3d atoms and nonmagnetic B atoms). Further, we proceed with a structural search for stable compounds and then study the stability of predicted antiferromagnetic (AFM) order by adding possible SF in the ground state (quantum zero-point motion). At the end, we estimate the influence of quantum SF on the possible appearance of SF induced superconductivity.

Crystal structures of Fe-Ni-B were searched by an adaptive genetic algorithm (AGA), which integrates auxiliary interatomic potentials and first-principles calculations together in an adaptive manner to ensure the high efficiency and accuracy (see the supplementary material for more details).[3,4] The structure searches were only constrained by the chemical composition, without any assumption on the Bravais lattice type, symmetry, atom basis, or unit cell dimensions. A range of different compositions around the FeNiB (111) compositional ratio (i.e., 211, 121, 112, 311, 131, 113, 221, 122, 212, 133, 313, 331, 321, 312,

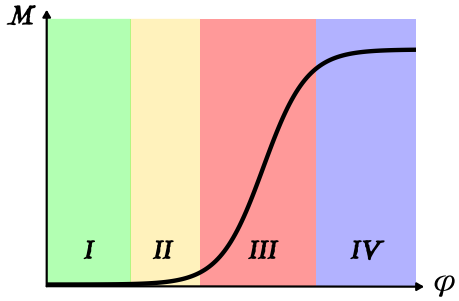

FIG. 1. Schematics of the HRS from a viewpoint of mean field description. Regions I and IV represent nonmagnetic and saturated regimes; region II corresponds to the quantum critical point, and a system in area III is in the HRS regime with possible large gradients of magnetization and strong spin fluctuations. *M* is the order parameter, while φ is the external perturbation (pressure, magnetic field, etc.).

123, 132, 231, 213, 223, 232, 322, 233, 323, and 332) were selected with 2 and 4 formula units to perform the AGA search. First-principles calculations were carried out using the projector augmented wave (PAW) method[5] within density functional theory (DFT) as implemented in the VASP code.[6,7] The exchange and correlation energy is treated within the spin-polarized generalized gradient approximation (GGA) and parameterized by the Perdew-Burke-Ernzerhof formula (PBE).[8] A plane-wave basis was used with a kinetic energy cutoff of 520 eV. During the AGA search, the Monkhorst–Pack sampling scheme[9] was adopted for Brillouin zone sampling with a *k*-point grid of $2\pi \times 0.033$ Å^{-1}, and the ionic relaxations stopped when the forces on every atom became smaller than 0.01 eV/Å. The energy convergence criterion is 10^{-4} eV. The phonon calculations were performed with the finite difference method via the Phonopy code.[10] The magnetic properties were calculated in a higher-quality calculation using a finer k-point sampling grid of spacing $2\pi \times 0.02$ Å^{-1} and a stricter energy convergence criterion of 10^{-6} eV.

Among all AGA searched ternary phases, a $FeNiB_2$ phase, with 2 formula units and a space group of $P2_1/m$ (space group number 11), is found to show the energy even smaller than the Gibbs triangle formed by the existing stable phases on the ternary phase diagram. The structure of this phase is shown in Fig. 2(a). There is one Wyckoff site for Fe and Ni and two Wyckoff sites for B (the crystallographic details are given in the supplementary material). The Fe, Ni, and B atoms formed a separated 1D zigzag chain. The phonon calculation further confirmed that the phase is dynamically stable without any soft phonon mode at $T = 0$ K, which is shown in Fig. 2(b).

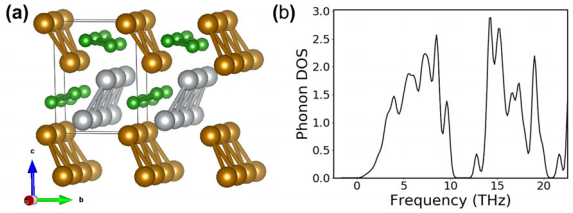

FIG. 2. (a) The configuration of $FeNiB_2$ from the AGA search. Atom color: Fe atoms colored with brown; Ni atoms colored with silver; and B atoms colored with green. (b) Phonon density of states.

With the predicted $FeNiB_2$ structure, the existing Fe-Ni-B phase diagram should be updated. In the current DFT-calculated database (i.e., the Materials Project[11]), there are eight reported binary stable phases; however, there is no ternary stable phase reported. It should be noted that while the experimental database (i.e., Inorganic Crystal Structure Database[12]) shows that a few ternary phases such as FeNiB, Fe_2NiB, $Fe_3Ni_3B_2$, and $Fe_3Ni_{20}B_6$ have been previously synthesized by experiments, they are all metastable phases according to DFT calculations, indicating that they may decompose to the surrounding stable phases on the Gibbs triangle in the equilibrium state.[13,14] The existing ternary convex hull computed from the DFT calculation is shown in Fig. 3(a) (the detailed energy values are provided in the supplementary material). At the composition of $FeNiB_2$, the thermodynamic stability is determined by the Gibbs triangle formed by the nearby Ni_4B_3, FeB, and FeB_2 phases. Considering the following reaction: $FeNiB_2 \rightarrow (Ni_4B_3 + 3FeB + FeB_2)/4$, $FeNiB_2$ is a stable phase if the formation energy on the left hand side is lower than that on the right hand side. The DFT calculations indeed show that the formation energy of $FeNiB_2$ in the $P2_1/m$ structure is equal to −340.9 meV/atom, while on the right-hand side, i.e., the energy on the convex hull at the composition of $FeNiB_2$ is calculated to be −326.57 meV/atom. Therefore, $FeNiB_2$ is thermodynamically stable at the temperature of 0 K and the convex hull of the Fe-Ni-B system should be updated with the inclusion of the $FeNiB_2$ phase. The updated phase diagram of the Fe-Ni-B system at 0 K is shown in Fig. 3(b).

Considering the stability of the $FeNiB_2$ phase, we search the literature to see if there is any hint of its existence. First, we find that the stable CoB phase (tetragonal, space group Pnma) shows the same motif as the current $FeNiB_2$ phase. From the chemical viewpoint, Co atoms should easily be replaced by Fe and Ni atoms. Moreover, while the ground state of FeB is the tetragonal phase ($I4_1/amd$), experiments always result in the metastable FeB analogous to the CoB structure, due to the vibrational properties as suggested in Ref. 15. Very interestingly, Gianoglio and Badini[14] reported that Ni can substitute Fe in the FeB-Pnma phase up to 70%. They showed that the lattice of 50%Ni substituted FeB was 0.40, 0.30, and 0.54 nm, which is consistent with our current results of 0.395, 0.30, and 0.532 nm except that the cell angle β becomes 91.35° in our DFT calculations (see the supplementary material for a detailed comparison). With these pieces

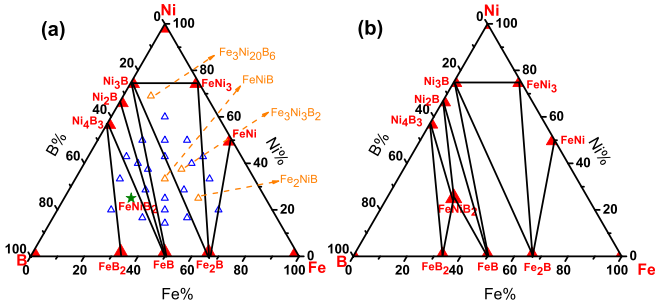

FIG. 3. DFT-calculated convex hull of the Fe-Ni-B system based on (a) previously reported phases and (b) after including the discovered $FeNiB_2$ phase. All DFT calculations were carried out at 0 K. Red solid triangles represent stable compounds and the green solid star represent the found stable phase, while blue and orange open triangles indicate the metastable phases from AGA search and experiments, respectively. The black lines separate the compositional space to Gibbs triangles.

of evidence, we believe that $FeNiB_2$ exists; however, it is not explicitly reported by experiments.

With the verified stability of the $FeNiB_2$ structure, we are now in a position to investigate its magnetic ground state. The DFT calculations are performed for the ferromagnetic (FM) state and the simplest AFM state, in which two Fe atoms in the primitive cell show opposite spin directions. It shows a strong competition of energetic stability between the FM and AFM states in the $FeNiB_2$ structure at 0 K. As shown in Fig. 4(a), the two states exhibit very similar energies, while the AFM state has a slightly lower energy of ~0.45 meV/atom at the equilibrium volume of 7.8 $Å^3$/atom. As the volume increases, the energy difference becomes larger and the AFM state is always slightly more stable than the FM state. More interestingly, in Fig. 4(b), the equilibrium magnetic moments demonstrate a rapid increase (nearly by 10 times). While the current results were based on a fixed geometry of the lattice, the calculation with relaxed structures shows almost the same results (see the supplementary material). By using the mean field approximation of the Heisenberg model, the Neel temperature is estimated to be nearly 50–60 K (the Heisenberg model parameters were calculated using Ref. 16). It suggests that the $FeNiB_2$ structure is located at the highly responsive state (region III in Fig. 1). The coexistence of different magnetic long-range orders, even for small values of atomic magnetic moments, indicates that the energy profile should have many local minima without well-defined global minimum. Correspondingly, the system is very sensitive to any external perturbation and could easily change its magnetic state ("magnetic chameleon") including magnetic tunneling. We note that this HRS can be a characterization of the $FeNiB_2$ phase compared to the analogous FeB-Pnma phase, which has a ferromagnetic ground state.

Let us now address the issue of magnetic instability. Our nonmagnetic calculations of $FeNiB_2$ revealed that the density of states (DOS) at the Fermi level is dominated by Fe electrons. So the Stoner criterion[17] is fulfilled,

$$1 - I\chi_0 > 0. \tag{1}$$

Here, χ_0 is the nonenhanced magnetic susceptibility, while I is the effective Stoner parameter of static local density approximation (LDA). For the multicomponent system, the corresponding Stoner criterion was obtained in Ref. 18 and is written as

$$N_t(E_F)I > 1 \quad \text{or} \quad \sum\nolimits_i I_i N_i^2 > N_t, \tag{2}$$

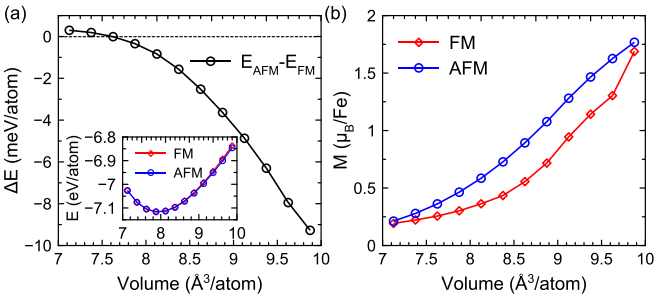

FIG. 4. (a) The energy difference and (b) the Fe magnetic moment in AFM and FM states as a function of the volume for the $FeNiB_2$ structure. The inset in (a) shows the total energies for both configurations.

where the effective Stoner parameter I for the multicomponent system is defined as $I = \sum_i I_i \left(\frac{N_i}{N_t}\right)^2$, where I_i and N_i are the partial Stoner parameter and partial DOS at the Fermi level, respectively, and N_t is the total DOS at the Fermi level. The obtained numbers are shown in Table I, and the resulting criteria of possible long-range AFM order are fulfilled. Such criteria are also fulfilled at many other q-vectors, including the FM one. We also found that criteria of a local magnetic moment stability (Anderson criteria[17,19]) are satisfied as well.

However, LDA traditionally overestimates the magnetism for weakly magnetic systems due to the neglect of quantum SF at $T = 0$ K (spin zero-point motion). To study the stability of the above predicted weak magnetism in $FeNiB_2$, we used a modified version of SF theory from Ref. 20. First, we obtain the *ab initio* SF energy (absent in LDA) using the random phase approximation (RPA) technique.[20,21] Then, we calculate the corresponding SF contribution to the spin susceptibility and finally obtain the renormalized Stoner criterion for magnetic instability.

The following RPA expression for the SF contribution to the total energy has been used:

$$\begin{aligned} E_{SF} &= \lim_{T\to 0} F_{SF} \\ &= 2\hbar \lim_{T\to 0} \sum\nolimits_\nu \int_0^I dI \int_{\Omega_{BZ}} d\boldsymbol{q} \int_{-\infty}^{\infty} d\omega (\mathrm{Im}\chi_\nu(\boldsymbol{q},\omega) \\ &\quad - \mathrm{Im}\chi_{\nu 0}(\boldsymbol{q},\omega))\coth(\beta\omega/2). \end{aligned} \tag{3}$$

This expression can also be rewritten as

$$E_{SF} = \frac{1}{2}\int_0^I dI\left(M^2 - M_0^2\right), \tag{4}$$

where M^2 is a square mean of magnetic moment obtained with enhanced and nonenhanced susceptibility (see Fig. 8 in Ref. 22 for the detailed definition and calculations of these quantities in pure 3d metals). Additional computational details of our linear response method can be found in Ref. 22.

The transverse part of SF correction to the inverse magnetic susceptibility is obtained directly as

$$\chi_{SF}^{-1} = \frac{1}{2M}\frac{\partial}{\partial M}\left(\int_0^I dI(\langle M^2\rangle - \langle M_0^2\rangle)\right). \tag{5}$$

This expression is different from the one used in Refs. 20 and 23 as we do not employ low frequency and long wavelength approximations.[24] The SF renormalized Stoner criterion then is written as

TABLE I. The partial density of states at the Fermi level and the Stoner parameter at each atom for $FeNiB_2$.

	DOS at E_f (state/eV)	I (eV)
Total (N_t)	1.962	…
Fe	1.477	0.84
Ni	0.312	0.87
B	0.0895	2.20

$$\left(\chi_{SF}^{-1}+\chi^{-1}\right)\chi_0 = 1 - I^*\chi_0 > 0, \quad (6)$$

where I^* is a renormalized Stoner parameter, which includes quantum spin zero points SF beyond usual static LDA. This renormalization was first noticed by Moriya and Kawabata[20] and studied recently using realistic electronic structure calculations in Ref. 23 for several simple 3d metals. All these studies have been performed using *ad hoc* low frequency and long wave approximations. Our approach is truly *ab initio* and takes into account SF at all q vectors and frequencies.

Our results indicated that the SF renormalization of the effective Stoner parameter in $FeNiB_2$ is nearly 7% with dominating suppression coming from Fe sites. Many different SFs with q-vectors around AFM instability contribute to this suppression in the frequency range up to 0.3 eV, but all electronic transitions inside electronic d-band (4–5 eV) contribute to this renormalization. It suggests that the existence of predicted low-frequency SF can be measured by neutron scattering experiments. Both longitudinal and transversal SFs on Ni sites are also strong, but due to small original static moment on Ni atoms, the Ni contribution to the total magnetization suppression is small.

The appearance of AFM-like magnetic instability can also be favorable for SF induced superconductivity. While s-wave and triplet superconductivity could theoretically appear near FM instability, such systems are not really known. Superconductivity reports in weakly FM system $ZnZr_2$ under pressure have not been confirmed. But more popular singlet superconductivity can naturally appear near AFM instability (cuprates[1] and iron pnictides[2]). So the appearance of superconductivity looks possible in this system, and now, we will estimate a strength of electron-spin interaction and its contribution to SF induced superconductivity.

From the practical point of view, e.g., for the search of superconducting material, the qualitative estimation of coupling constant λ is of primary interest. To obtain the required strength of spin-electron interaction, we will use the well known s-d exchange model.[25] To estimate λ, we do not need to consider the superconducting phase since it enters just the mass renormalization in the normal state and one needs just to deal with the corresponding expression for the electron self-energy,[25]

$$\Sigma_k(E) = I^2\sum_q \int_0^\infty \frac{d\omega}{4\pi} Im\chi(\boldsymbol{k}-\boldsymbol{q},\omega)\left[\frac{1-f_q}{E-\varepsilon_q-\omega}+\frac{f_q}{E-\varepsilon_q+\omega}\right], \quad (7)$$

where f_q is the Fermi distribution with ε_q being one electron spectrum. The expression for the coupling constant at $T=0$ K is then written in the standard way as

$$\lambda = -\left.\frac{\partial\langle\Sigma_k(E)\rangle}{\partial E}\right|_{E=0}. \quad (8)$$

To make the simplest possible estimation of electron-magnon interaction, one can replace the average over the Fermi surface above by the average over the Brillouin zone. To further obtain the temperature of the superconducting transition using the approach advocated above, we use the usual MacMillan formula.[26] Under these approximations, our calculated value is $\lambda = 0.6$ and the effective SF frequency is $\omega = 0.2$ eV. With these numbers, we obtain a value of 20–30 K for the critical temperature. Thus, our qualitative estimation predicts not only suppression of magnetic long-range order in the normal state but also suggests a very promising scenario for the SF induced superconductivity near the AFM quantum critical point.

In summary, we performed a structure search for a stable system near magnetic instability. Our AGA approach that integrates auxiliary interatomic potentials and first-principles calculations found a stable compound $FeNiB_2$, which appears to be a magnetically highly responsive system close to antiferromagnetic instability. The structure of $FeNiB_2$ is analogous to the FeB-Pnma phase, and the previous literature provides hints of its possible existence. Compared to the ferromagnetic long-range order of FeB, this system is characterized by strong anti-ferromagnetic-like spin fluctuations at T = 0 K (quantum spin zero-point motion) and possible spin fluctuation induced superconductivity. The experimental verifications of our prediction are highly desirable. Our magneto-structural combined studies thus open a promising route for the search of strong SF states and superconductors.

See the supplementary material for the details of the AGA method, the crystallographic data of $FeNiB_2$, the structure database of the Fe-Ni-B system, the construction of the ternary convex hull, the comparison between FeB and $FeNiB_2$, and some details of magnetic calculations.

The work at the Ames Laboratory was supported by the U.S. Department of Energy, Basic Energy Sciences, Materials Science and Engineering Division, under Contract No. DEAC02-07CH11358, including a grant of computer time at the National Energy Research Scientific Computing Center (NERSC) in Berkeley, CA. The work at the University of Science and Technology of China was supported by the National Natural Science Foundation of China (Nos. 11574284 and 11774324) and the Supercomputing Center of the University of Science and Technology of China. R. Wang acknowledges the support from China Scholarship Council (File No. 201906340034).

REFERENCES

[1]T. Moriya and K. Ueda, Adv. Phys. **49**, 555 (2000).
[2]D. C. Johnston, Adv. Phys. **59**, 803 (2010).
[3]S. Q. Wu, M. Ji, C. Z. Wang, M. C. Nguyen, X. Zhao, K. Umemoto, R. M. Wentzcovitch, and K. M. Ho, J. Phys.: Condens. Matter **26**, 035402 (2014).
[4]X. Zhao, M. C. Nguyen, W. Y. Zhang, C. Z. Wang, M. J. Kramer, D. J. Sellmyer, X. Z. Li, F. Zhang, L. Q. Ke, V. P. Antropov, and K. M. Ho, Phys. Rev. Lett. **112**, 045502 (2014).
[5]P. E. Blöchl, Phys. Rev. B **50**, 17953 (1994).
[6]G. Kresse and J. Furthmüller, Comput. Mater. Sci. **6**, 15 (1996).
[7]G. Kresse and J. Furthmüller, Phys. Rev. B **54**, 11169 (1996).
[8]J. P. Perdew, K. Burke, and M. Ernzerhof, Phys. Rev. Lett. **77**, 3865 (1996).
[9]H. J. Monkhorst and J. D. Pack, Phys. Rev. B **13**, 5188 (1976).
[10]A. Togo and I. Tanaka, Scr. Mater. **108**, 1 (2015).
[11]A. Jain, S. P. Ong, G. Hautier, W. Chen, W. D. Richards, S. Dacek, S. Cholia, D. Gunter, D. Skinner, G. Ceder, and K. A. Persson, APL Mater. **1**, 011002 (2013).
[12]M. Hellenbrandt, Crystallogr. Rev. **10**, 17 (2004).
[13]Y. Khan, Z. Metallkd. **74**, 385 (1983); available at https://www.tib.eu/en/search/id/tema-archive%3ATEMAW83002944UDM/Crystallization-behaviour-of-the-melt-quenched/.
[14]C. Gianoglio and C. Badini, J. Mater. Sci. **21**, 4331 (1986).

[15]A. N. Kolmogorov, S. Shah, E. R. Margine, A. F. Bialon, T. Hammerschmidt, and R. Drautz, Phys. Rev. Lett. **105**, 217003 (2010).
[16]A. I. Liechtenstein, M. I. Katsnelson, V. P. Antropov, and V. A. Gubanov, J. Magn. Magn. Mater. **67**, 65 (1987).
[17]G. D. Samolyuk and V. P. Antropov, Phys. Rev. B **79**, 052505 (2009).
[18]T. Jarlborg and A. J. Freeman, Phys. Rev. B **22**, 2332 (1980).
[19]P. W. Anderson, Phys. Rev. **124**, 41 (1961).
[20]T. Moriya and A. Kawabata, J. Phys. Soc. Jpn. **34**, 639 (1973).
[21]F. Englert and R. Brout, Phys. Rev. **120**, 1085 (1960).
[22]A. L. Wysocki, V. N. Valmispild, A. Kutepov, S. Sharma, J. K. Dewhurst, E. K. U. Gross, A. I. Lichtenstein, and V. P. Antropov, Phys. Rev. B **96**, 184418 (2017).
[23]V. P. Antropov and A. Solontsov, J. Appl. Phys. **109**, 07E116 (2011).
[24]V. P. Antropov, J. Magn. Magn. Mater. **262**, L192 (2003).
[25]V. Y. Irkhin and M. I. Katsnelson, Z. Phys. B **75**, 67 (1989).
[26]W. L. McMillan, Phys. Rev. **167**, 331 (1968).

Supplementary Material for "Theoretical prediction of a highly responsive material: spin fluctuations and superconductivity in $FeNiB_2$ system"

Renhai Wang[1,2], Yang Sun[2*], Vladimir Antropov[2*], Zijing Lin[1], Cai-Zhuang Wang[2,3], Kai-Ming Ho[2,3,4]

[1]Department of Physics, University of Science and Technology of China, Hefei 230026, China

[2]Ames Laboratory, US DOE, Ames, Iowa 50011, USA

[3]Department of Physics, Iowa State University, Ames, Iowa 50011, USA

[4]International Center for Quantum Design of Functional Materials (ICQD), Hefei National Laboratory for Physics Sciences at the Microscale, University of Science and Technology of China, Hefei 230026, China

Content

S1. Adaptive genetic algorithm (AGA) method

In the AGA search[1], energy was used as the selection criteria for optimizing the candidate structure pool. The pool size of candidate structure in GA search was 128. At each GA generation, 32 structures were generated from the parent structure pool via the mating procedure described in[2]. The structures in the pool were updated by keeping the 128 lowest-energy structures. The structure search with a given auxiliary interatomic potential sustained 600 consecutive GA generations. 16 structures from the GA search were randomly selected for first-principles calculations to re-adjust the potential parameters of the auxiliary classical potential for the next round of the GA search. The adaptive iterations were repeated 40 times.

For the search of Fe-Ni-B system, interatomic potentials based on the embedded-atom method (EAM)[3] were chosen as the auxiliary classical potential. In EAM, the total energy of an *N*-atom system was described by

$$E_{total} = \frac{1}{2}\sum_{i,j(i\neq j)}^{N} \phi(r_{ij}) + \sum_i F_i(n_i), \quad \text{(S1)}$$

where $\phi(r_{ij})$ is the pair term for atoms i and j at distance r_{ij}. $F_i(n_i)$ is the embedded term with electron density term $n_i = \sum_{j\neq i} \rho_j(r_{ij})$ at the site occupied by atom i. The fitting parameters in the EAM formula was chosen as follows: The parameters for Fe-Fe and Ni-Ni interactions were taken from the literature[4]. Other pair interactions (B-B, Fe-Ni, Fe-B and B-Ni) were modeled by Morse function,

$$\phi(r_{ij}) = D\left[e^{-2\alpha(r_{ij}-r_0)} - 2e^{-\alpha(r_{ij}-r_0)}\right], \quad \text{(S2)}$$

where D, α, r_0 are fitting parameters. The density function for B atoms were modeled by an exponential decaying function

$$\rho(r_{ij}) = \alpha\, exp\left[-\beta(r_{ij} - r_0)\right], \quad \text{(S3)}$$

where α and β are fitting parameters. The form proposed by Benerjea and Smith[5] was used as the embedding function with fitting parameters F_0, γ as

$$F(n) = F_0[1 - \gamma\, In\, n]n^{\gamma}. \quad \text{(S4)}$$

For Fe and Ni, the parameters of the density function and embedding function were taken from Ref.[4]. Other parameters were adjusted adaptively by fitting to the DFT energies, forces, and stresses of selected structures in the AGA scheme[1]. The fitting process was performed by the force-matching method with stochastic simulated annealing algorithm implemented in the *potfit* code[6,7].

S2. Crystallographic data of stable $FeNiB_2$.

Table S1 Crystallographic data of $FeNiB_2$.

Space group	Lattice parameters	Atoms	Atomic coordinates		
			x	y	z
$P2_1/m$	a=3.95 Å	Fe	0.377	0.25	0.179
	b=3.00 Å	Ni	0.119	0.25	0.676
	c=5.32 Å	B	0.614	0.25	0.536
	α=γ=90°, β=91.35°	B	0.878	0.25	0.028

S3. Structure database for Fe-Ni-B system

To characterize the energetic stability of structures at different compositions obtained by AGA search, the formation energy (E_f) of any given structure $Fe_mNi_nB_p$ was calculated by:

$$E_f = \frac{E(Fe_mNi_nB_p) - mE(Fe) - nE(Ni) - pE(B)}{m+n+p}, \quad \text{(S5)}$$

where $E(Fe_mNi_nB_p)$ is the total energy of the $Fe_mNi_nB_p$. $E(Fe)$, $E(Ni)$ and $E(B)$ are the per-atom energy of bulk Fe, Ni and B in the reference structures, which are cubic (BCC) Fe, face-centered cubic (FCC) Ni and rhombohedral *R*-3*m* B, respectively.

During the search with different compositions, we used the following method to judge the stability of a compound: For any ternary compound $A_xB_yC_z$ and any three compounds ($A_{x1}B_{y1}C_{z1}$, $A_{x2}B_{y2}C_{z2}$, and $A_{x3}B_{y3}C_{z3}$), if $A_xB_yC_z$ can be balanced to $a*A_{x1}B_{y1}C_{z1} + b*A_{x2}B_{y2}C_{z2} + c*A_{x3}B_{y3}C_{z3}$ in the condition a >= 0, b >= 0 and c >=0, the formation energy E_F is calculated as $E_F=E(A_xB_yC_z) - a*E(A_{x1}B_{y1}C_{z1}) - b*E(A_{x2}B_{y2}C_{z2}) - c*E(A_{x3}B_{y3}C_{z3})$. If the E_F is always less than zero with any references including pure elements, binary and ternary phases, the $A_xB_yC_z$ is energetically stable.

All experimental phases and the AGA searched stable phases, including the symmetry, lattice parameters, formation energies relative to the pure Fe, Ni, B phases, and formation energies above convex hull, are listed in Table S2. Experimentally obtained metastable phases and the AGA searched metastable phases are listed in Table S3.

Table S2 Structure database for Fe-Ni-B convex-hull. The formation energy E_f (meV/atom) are referenced to pure Fe, Ni and B. The formation energy H (meV/atom) are referenced to the stable phases that formed Gibbs triangle. All phases in bold are thermodynamic stable phases and are used to construct the convex hull.

	Phases	Symmetry	a (Å)	b (Å)	c (Å)	α, β, γ	E_f	H
Existing stable phases	**Fe**	*Im*-3*m*	2.83	2.83	2.83	90.0, 90.0, 90.0	0	**0**
	Ni	*Fm*-3*m*	3.51	3.51	3.51	90.0, 90.0, 90.0	0	**0**
	B	*R*-3*m*	4.89	4.89	12.56	90.0, 90.0, 120.0	0	**0**
	FeNi	*P*4/*mmm*	2.51	2.51	3.57	90.0, 90.0, 90.0	-70.5	**0**
	$FeNi_3$	*Pm*-3*m*	3.53	3.53	3.53	90.0, 90.0, 90.0	-91.9	**0**
	FeB	$I4_1/amd$	2.93	2.93	14.95	90.0, 90.0, 90.0	-387.2	**0**
	Fe_2B	*I*4/*mcm*	5.05	5.05	4.22	90.0, 90.0, 90.0	-321.3	**0**
	FeB_2	*Pnma*	4.81	4.80	3.74	90.0, 90.0, 90.0	-307.4	**0**
	Ni_4B_3	*Pnma*	3.00	6.57	11.97	90.0, 90.0, 90.0	-282.8	**0**
	Ni_2B	*I*4/*mcm*	4.11	4.11	4.11	90.0, 90.0, 90.0	-293.4	**0**
	Ni_3B	*Pnma*	4.39	5.20	6.63	90.0, 90.0, 90.0	-263.9	**0**
	Ni_2B	*I*4/*mcm*	4.11	4.11	4.11	90.0, 90.0, 90.0	-292.1	**0**
GA-found stable phase	**$FeNiB_2$**	$P2_1/m$	3.95	3.0	5.32	90.0, 91.35, 90.0	-340.9	**0**

Table S3 AGA metastable structure database of Fe-Ni-B system. The formation energy H (meV/atom) are referenced to the stable phases that formed Gibbs triangle.

	Phases	Symmetry	a (Å)	b (Å)	c (Å)	α, β, γ	E_f	H
Existing metastable phases	FeNiB	*Fmmm*	4.19	7.04	7.19	90.0, 90.0, 90.0	-258.1	52.3
	Fe_2NiB	*Pnma*	5.32	6.58	4.42	90.0, 90.0, 90.0	-214.4	49.6
	$Fe_3Ni_3B_2$	$P2_1$	4.42	5.28	6.62	90.0, 90.05, 90.0	-215.9	48.0
	$Fe_3Ni_{20}B_6$	*Fm*-3*m*	10.44	10.44	10.44	90.0, 90.0, 90.0	-232.9	1.41
GA-found metastable phases	FeNiB	*Pnma*	5.47	3.14	6.34	90.0, 90.0, 90.0	-269.1	41.3
	Fe_2NiB	*C2/m*	14.60	3.00	8.56	90.0, 123.9, 90.0	-187.7	76.2
	$FeNi_2B$	*Cmcm*	2.88	8.13	6.55	90.0, 90.0, 90.0	-206.8	57.1
	Fe_3NiB	*P*-1	6.26	6.31	6.50	83.4, 65.3, 60.8	-73.3	147.6
	$FeNi_3B$	*P*-1	5.27	6.28	6.70	100.8, 113.2, 90.0	-167.7	61.9
	$FeNiB_3$	*P*1	4.83	5.01	7.87	77.5, 88.3, 87.5	-6.91	276.5
	Fe_2Ni_2B	*P*-1	6.29	6.35	6.58	106.2, 102.0, 118.4	-101.0	128.5
	$FeNi_2B_2$	*P*-1	4.85	5.61	6.83	82.6, 88.0, 73.8	-169.3	161.6
	Fe_2NiB_2	*P4/mbm*	5.60	5.60	5049	90.0, 90.0, 90.0	-200.5	140.6
	Fe_3Ni_2B	*Cc*	6.84	10.16	7.60	90.0, 109.8, 90.0	-62.3	140.7
	Fe_3NiB_2	*C2/m*	11.21	5.80	7.64	90.0, 117.7, 90.0	-184.4	131.5
	$FeNi_2B_3$	*Cc*	15.09	5.33	4.92	90.0, 101.4, 90.0	-227.1	85.6
	$FeNi_3B_2$	*Cm*	10.71	6.37	8.28	90.0, 130.2, 90.0	-242.2	62.8
	$FeNi_3B_3$	*P-1*	4.00	5.50	6.15	103.9, 108.0, 101.4	-249.0	71.6
	Fe_2NiB_3	*P-1*	4.93	5.86	7.20	89.0, 75.6, 72.5	-288.6	67.7
	$Fe_3Ni_3B_2$	*P1*	6.06	6.74	8.55	91.6, 90.0, 116.7	-166.9	97.1
	Fe_2Ni_3B	*C2/m*	16.60	2.56	6.19	90.0, 111.7, 90.0	-132.6	74.0
	$Fe_2Ni_2B_3$	*P1*	4.63	5.61	5.62	111.0, 105.6, 105.4	-183.7	163.3
	$Fe_2Bi_3B_2$	*C2/c*	11.14	4.46	5.41	90.0, 98.6, 90.0	-221.3	67.2
	$Fe_2Ni_3B_3$	*P-1*	4.66	6.13	6.20	117.7, 92.5, 111.0	-236.4	89.2
	Fe_3NiB_3	*R3*	8.40	8.40	5.87	90.0, 90.0, 120.0	-209.6	144.7
	Fe_3Ni_3B	*C2/m*	18.77	2.55	6.22	90.0, 100.1, 90.0	-85.7	104.5
	$Fe_3Ni_2B_3$	*P1*	4.85	5.68	5.69	90.2, 106.9, 106.6	-206.1	123.6
	$Fe_3Ni_2B_2$	*P-1*	4.40	5.71	6.04	76.2, 69.1, 70.8	-205.3	83.3

S4. Construction of the ternary convex hull

In a ternary system, the compositional space is combined by multiple regular triangular piece as shown in Fig. 3 in the main text. The convex hull is then composed of planes connecting the formation energies of all possible three stable phases. The surface formed by the bottom pieces of planes at any composition is the convex hull surface. The formation energies of all known stable structures are located on the surface of this convex cladding. Any structure having formation energy below this convex hull surface will be a stable structure and the convex hull surface will be re-constructed by considering the formation energy of the discovered structure.

S5. Comparison between FeB and $FeNiB_2$

In the Fig. S1(a), the $FeNiB_2$ structure is compared with Pnma-FeB. They are very similar except a slight difference of the lattice angle. Given the similarity between Pnma-FeB and $FeNiB_2$, one may need highly accurate X-ray diffraction (XRD) to differentiate them, as shown in Fig. S1(b). Meanwhile, we note FeB-Pnma is ferromagnetic state while current $FeNiB_2$ is a highly responsive state with strong competition between ferromagnetic and anti-ferromagnetic states. A detailed experimental characterization of magnetic properties of $FeNiB_2$ will therefore be very interesting.

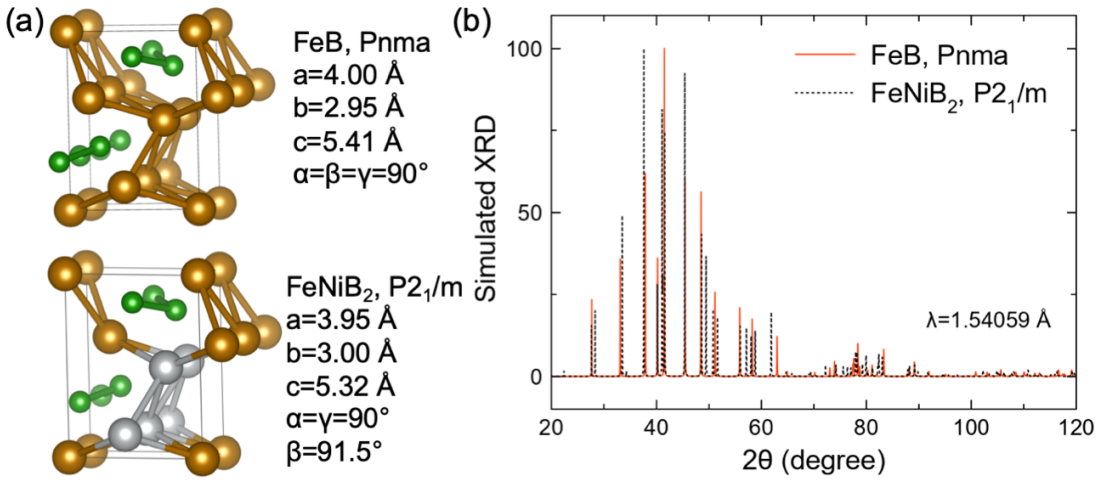

Fig. S1 (a) The structures and (b) simulated XRD patterns of Pnma-FeB and $P2_1/m$-$FeNiB_2$.

S6. Details of magnetic calculations

In this section we check the magnetic calculations for both relaxed structure and the structure without any relaxation (linear scaling of equilibrium lattice parameter while keeping all angles same). As shown in Fig. S2, while the relaxation caused small energy changes at large volume expansion, the two methods lead to almost same conclusions: (1) ferromagnetic (FM) and anti-ferromagnetic (AFM) states exhibit almost similar energies difference near equilibrium volume; (2) The magnetic moments shows a rapid increase with the lattice expansion.

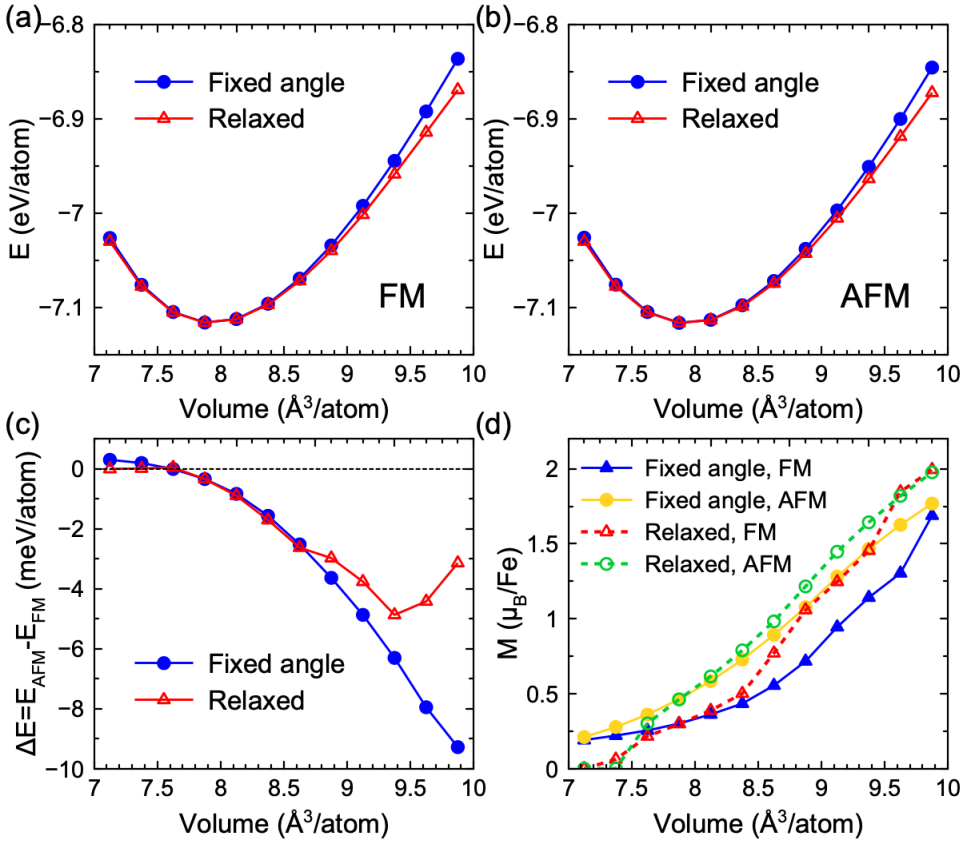

Fig. S2 The energy-volume curve for fixed lattice and relaxed structure with (a) ferromagnetic state and (b) anti-ferromagnetic state. (c) The energy differences between anti-ferromagnetic and ferromagnetic states as a function of volume for fixed lattice and fully relaxed structure. (d) The magnetic moment of Fe atoms as a function of volume in the different conditions.

However, we also notice a few differences between two methods: (1) at small volume (<7.5), the relaxations lead to a paramagnetic state no matter the initial state is FM or AFM; (2) at large volume (>9), the energy difference shows a non-smooth change. By checking the relaxed structures, we found it was due to the fact that the lattice angle β in the relaxed AFM and FM

structures converged to different values and followed different trends as shown in Fig. S3. To isolate the effect of magnetic configuration without considering the effect from geometric changes, we used the fixed geometric structure in the main text.

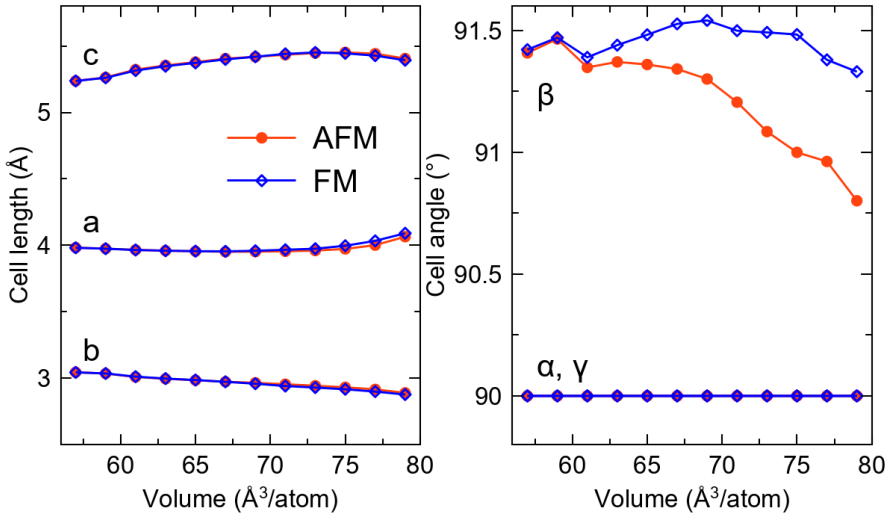

Fig. S3 The fully relaxed cell length and cell angles as a function of the volume.

References

[1] S.Q. Wu, M. Ji, C.Z. Wang, M.C. Nguyen, X. Zhao, K. Umemoto, R.M. Wentzcovitch, and K.M. Ho, J. Phys. Condens. Matter **26**, 035402 (2014).

[2] D.M. Deaven and K.M. Ho, Phys. Rev. Lett. **75**, 288 (1995).

[3] S.M. Foiles, M.I. Baskes, and M.S. Daw, Phys. Rev. B **33**, 7983 (1986).

[4] X.W. Zhou, R.A. Johnson, and H.N.G. Wadley, Phys. Rev. B - Condens. Matter Mater. Phys. **69**, 1 (2004).

[5] A. Banerjea and J.R. Smith, Phys. Rev. B **37**, 6632 (1988).

[6] P. Brommer and F. Gähler, Philos. Mag. **86**, 753 (2006).

[7] P. Brommer and F. Gähler, Model. Simul. Mater. Sci. Eng. **15**, 295 (2007).